Journal of Computational Physics **149,** 306–332 (1999)
Article ID jcph.1998.6155, available online at http://www.idealibrary.com on IDEAL®

Galerkin Spectral Method for the Vorticity and Stream Function Equations

F. Auteri* and L. Quartapelle†

**Dipartimento di Ingegneria Aerospaziale, Politecnico di Milano, Via Lambruschini, 15, 20156 Milano, Italy;*
†*Dipartimento di Fisica, Politecnico di Milano, Piazza Leonardo da Vinci, 32, 20133 Milano, Italy*
E-mail: *auteri@aero.polimi.it

Received July 13, 1998; revised October 29, 1998

A Galerkin–Legendre spectral method for the solution of the vorticity and stream function equations in uncoupled form under no-slip conditions in a square domain is presented which fully exploits the separation of variables in the two elliptic problems, benefits from a nonsingular influence matrix, and is able to solve the singular driven cavity problem (modulo Gibbs' phenomenon) even without regularizing the boundary condition at the corners.

Key Words: Galerkin–Legendre spectral methods; Navier–Stokes equations; Glowinski–Pironneau method.

1. INTRODUCTION

The use of the influence matrix is very common in the solution of the incompressible Navier–Stokes equations by means of spectral methods. This technique was introduced in the context of the 1D equations for plane channel flows by Kleiser and Schumann for the velocity/pressure formulation [14] and by Dennis and Quartapelle for the vorticity/stream function formulation as a means of satisfying conditions of an integral character for the vorticity [6]. Uncoupled solution methods based on the influence matrix can however face difficulties when applied to problems with two or three nonperiodic spatial directions. For instance, the influence matrix evaluated for *tau* or collocation Chebyshev spectral approximations to ω-ψ equations is found to possess a number of singularities related to the corners of a rectangular domain, see Ehrenstein and Peyret [7] and the recent review [16]. The difficulty of evaluating the value of vorticity on the corners is encountered also in the Chebyshev *tau*-method for the vorticity and velocity equations for 2D incompressible flows proposed by Clercx [5]. On the other hand, the collocation method proposed by Nguyen, Paik, and Chung [15] for solving the ω-ψ equations with two nonperiodic directions, by enforcing the 2D vorticity integral conditions [17] through the explicit construction of the

0021-9991/99 $30.00

harmonic functions required therein, does not suffer from any spurious singularity of the influence matrix. Unfortunately, this method prevents a full exploitation of the direct product structure of the two-dimensional problem and of its discrete representation by means of a spectral approximation.

Recently, the development of spectral methods has witnessed a trend toward the use of the Galerkin method to exploit the well known advantages stemming from the variational formulation of boundary value problems for elliptic operators, see, e.g., [2, 19]. In particular, fast elliptic Poisson spectral solvers using diagonalization techniques within the context of the standard Galerkin method have been developed by Shen using Legendre [21] or Chebyshev [22] polynomials. Therefore, these new spectral solution algorithms should allow us to reanalyze the issue of the singular nature of spectral influence matrices for the calculation of incompressible viscous flows.

The aim of this paper is to describe a Galerkin–Legendre method for the uncoupled solution of the vorticity and stream function equations in which the influence matrix for the determination of the vorticity boundary value is free from any singular behaviour. The method is based on imposing conditions of an integral kind for the vorticity according to an adaptation of the Glowinski–Pironneau method [8] to the considered spectral approximation. A distinctive feature of the proposed method is its capability of fully exploiting the separation of variables in the two underlying elliptic problems. The resulting solution algorithm for the 2D Navier–Stokes equations is characterized by a nonsingular influence matrix for which we are able to devise an uncoupling of the even–odd components of the vorticity trace fully compatible with the inclusion of the corner values. The proposed algorithm is found to be able to solve the singular driven cavity problem, but for an expected Gibbs' phenomenon, even without regularizing the boundary condition at the corners.

The content of the paper is organized as follows. In Section 2 we describe the Legendre basis proposed by Shen [21] for the approximation of ordinary differential operators and give the explicit representation of the spectral matrices of the second- and first-order derivatives as well as of the mass matrix, including the modes required to impose nonhomogeneous boundary conditions.

Section 3 is devoted to the study of the spectral solution of the 2D Helmholtz equation under possibly nonhomogeneous Dirichlet conditions, by means of the Galerkin–Legendre formulation. The problem is stated in Subsection 3.1. The treatment of the Dirichlet boundary data over a rectangular domain is described in Subsection 3.2 by recalling the concept of lifting the nonzero boundary values. More precisely, such a lifting is performed in two successive steps, the first one to account for the data specified at the corners and the second one to account for the boundary values prescribed in the interior of the sides. Then, in Subsection 3.3 we introduce a direct solution algorithm based on a bidiagonalization technique which relies on the eigenstructure of the mass matrices associated with the two spatial directions instead of the more common method of solving the eigenproblems of the second-derivative operators. The accuracy of the solution algorithm is assessed by some numerical tests and comparisons in Subsection 3.4

In Section 4 the spectral solution of the 2D Navier–Stokes equations in the vorticity and stream function formulation is addressed. First, we introduce the uncoupled solution method based on integral conditions for the vorticity (Subsection 4.1), second we describe the influence matrix technique to enforce these global conditions in a Legendre spectral context (Subsection 4.2) including the uncoupling of the even/odd modes of the trace, then we analyze how the nonlinear term can be dealt with according to the classical pseudospectral

technique (Subsection 4.3), and finally we show some numerical results for the (unregularized) driven cavity problem, for both steady and unsteady solutions (Subsection 4.4). The last section is devoted to a few concluding remarks.

2. GALERKIN–LEGENDRE APPROXIMATION

In this section, the Galerkin–Legendre approximation in one dimension is considered and the explicit form of the stiffness and mass matrix is given, following the derivation of Shen [21] and including the treatment of nonhomogeneous boundary conditions at the interval extremes.

Let us consider the basis for representing functions of x defined on the interval $[-1, 1]$,

$$\{L_n^*(x), 0 \le n \le N\} \equiv \left\{1, x/\sqrt{2}, k_{n-1}(1-x^2)L'_{n-1}(x), 2 \le n \le N\right\},$$

where $k_n \equiv (\sqrt{n+1/2})/(n+n^2)$ and $L_n(x)$, $n = 0, 1, \ldots$, are the Legendre polynomials. Thus $L_n^*(x)$ is a polynomial of degree n for any $n \ge 0$ and, for $n \ge 2$, one has Shen's basis [21]

$$L_n^*(x) = \frac{L_{n-2}(x) - L_n(x)}{\sqrt{2(2n-1)}}, \qquad n \ge 2.$$

The normalization of $L_n^*(x)$ for $n > 0$ has been chosen to make the stiffness matrix coincident with the unit matrix of proper dimension, but for the constant mode. In fact, once the stiffness matrix D is defined by

$$d_{n,k} \equiv \int_{-1}^{1} L_n^*(x)' \, L_k^*(x)' \, dx, \qquad n, k \ge 0,$$

it is immediate to see that

$$\begin{aligned} d_{n,k} &= \delta_{n,k}, \qquad n, k \ge 1, \\ d_{n,0} &= d_{0,n} = 0, \qquad n \ge 0, \end{aligned}$$

as a consequence of the Sturm–Liouville equation for Jacobi polynomials and of the normalization

$$\int_{-1}^{1} L_n(x) L_k(x) \, dx = \frac{2}{2n+1} \delta_{n,k}, \qquad n, k \ge 0.$$

For further reference, the $(N+1) \times (N+1)$ stiffness matrix is denoted by ${}^0D$ to emphasize that its leading element $D_{0,0}$ is zero; namely, we write

$${}^0D = \begin{array}{c} \\ 0 \\ 1 \\ 2 \\ \vdots \\ N \end{array} \begin{array}{c} \begin{array}{ccccc} 0 & 1 & 2 & \cdots & N \end{array} \\ \begin{pmatrix} 0 & & & & \\ & 1 & & & \\ & & 1 & & \\ & & & \ddots & \\ & & & & 1 \end{pmatrix} \end{array}.$$

Similarly, the $(N+1)\times(N+1)$ mass matrix M is defined by

$$m_{n,k} \equiv \int_{-1}^{1} L_n^*(x)\, L_k^*(x)\, dx, \qquad n,k \geq 0.$$

By elementary properties of Jacobi polynomials or as demonstrated in [21], the only nonzero elements of M are located along the diagonal and two codiagonals, according to the penta-diagonal profile

$$M = \begin{array}{c} \\ 0 \\ 1 \\ 2 \\ 3 \\ 4 \\ \vdots \\ N-2 \\ N-1 \\ N \end{array} \begin{array}{c} \begin{array}{ccccccccc} 0 & 1 & 2 & 3 & 4 & \cdots & N-2 & N-1 & N \end{array} \\ \begin{pmatrix} c_0 & 0 & a_0 & & & & & & \\ 0 & c_1 & 0 & a_1 & & & & & \\ a_0 & 0 & c_2 & 0 & a_2 & & & & \\ & a_1 & 0 & c_3 & 0 & \ddots & & & \\ & & a_2 & 0 & c_4 & 0 & \ddots & & \\ & & & \ddots & 0 & \ddots & 0 & a_{N-3} & \\ & & & & \ddots & 0 & c_{N-2} & 0 & a_{N-2} \\ & & & & & a_{N-3} & 0 & c_{N-1} & 0 \\ & & & & & & a_{N-2} & 0 & c_N \end{pmatrix} \end{array}.$$

A direct calculation gives

$$a_0 = \sqrt{\frac{2}{3}}, \qquad a_1 = \frac{1}{3\sqrt{5}}, \qquad a_n = \frac{-1}{(2n+1)\sqrt{(2n-1)(2n+3)}}, \qquad n \geq 2,$$

$$c_0 = 2, \qquad c_1 = \frac{1}{3}, \qquad c_n = \frac{2}{(2n-3)(2n+1)}, \qquad n \geq 2.$$

For completeness, we give also the matrix B expressing the Legendre approximation of the first derivative, namely, the coefficients

$$b_{n,k} \equiv \int_{-1}^{1} L_n^*(x)\, L_k^*(x)'\, dx, \qquad n,k \geq 0.$$

In this case, one finds that the only nonzero elements of B are located along the two codiagonals nearest to the diagonal, as

$$B = \begin{array}{c} \\ 0 \\ 1 \\ 2 \\ 3 \\ 4 \\ \vdots \\ N-1 \\ N \end{array} \begin{array}{c} \begin{array}{ccccccccc} 0 & 1 & 2 & 3 & 4 & \cdots & N-1 & N \end{array} \\ \begin{pmatrix} 0 & \hat{b} & & & & & & \\ 0 & 0 & \tilde{b} & & & & & \\ & \overline{b} & 0 & b_2 & & & & \\ & & -b_2 & 0 & b_3 & & & \\ & & & -b_3 & 0 & \ddots & & \\ & & & & -\ddots & \ddots & b_{N-2} & \\ & & & & & -b_{N-2} & 0 & b_{N-1} \\ & & & & & & -b_{N-1} & 0 \end{pmatrix} \end{array}.$$

A direct calculation gives

$$\hat{b} = \sqrt{2}, \qquad \tilde{b} = \frac{1}{2\sqrt{3}}, \qquad \bar{b} = \frac{1}{\sqrt{3}},$$
$$b_n = \frac{1}{\sqrt{4n^2 - 1}}, \qquad n \geq 2.$$

Note that matrix B is antisymmetric only when it is restricted to the range $(n, k) \geq 2$.

3. HELMHOLTZ EQUATION

The prototype algorithm for solving Poisson and Helmholtz equations in a rectangle by spectral methods is the diagonalization technique proposed in [9, p. 150]. This algorithm has been implemented by Haidvogel and Zang using Chebyshev polynomials and the *tau* method [12]. Recently, a diagonalization algorithm for the direct solution of the Galerkin variational approximation of elliptic equations by Legendre polynomials has been introduced by Shen [21].

In this section we describe an algorithm based on diagonalization for the solution of a Helmholtz equation supplemented by a nonhomogeneous Dirichlet condition. A distinctive feature of the method to be described is that it exploits the direct-product structure of the spectral approximation in all its algorithmic components, including the lifting of the nonzero boundary data which is the most appropriate way to account for a nonzero Dirichlet condition within a variational framework. As explained for instance in Strang and Fix [23, pp. 70, 199–203], the lifting consists in subtracting to the unknown a conveniently smooth function whose trace is equal to the prescribed nonzero boundary value and which is, for the rest, completely arbitrary.

The content of this section is organized as follows. First, the spectral approximation is applied to the solution of the Dirichlet problem for the Helmholtz operator. Then, a detailed analysis of the lifting necessary to impose the nonhomogeneous Dirichlet condition at the discrete level is given. The form assumed by the discrete lifting is such that the Dirichlet boundary values are accounted for in an original fashion by solving a mass matrix problem for each side. The values of the Dirichlet datum at the four corners are employed by the algorithm together with the values at the Gauss–Legendre points of each side. A bidiagonalization algorithm for the efficient solution of a Helmholtz equation in a rectangular domain is proposed along lines very similar to Shen's algorithm [21], namely, with the diagonalization process based on the eigenstructure of the mass matrix, instead of that for the second-order derivative operator expressed either in a weak or collocation form. On the other hand, differently from Shen's algorithm we use the diagonalization in both spatial directions. Finally, some numerical tests of the new direct spectral solver are presented.

3.1. Spectral Solution of the Helmholtz Equation

Let us consider the Dirichlet problem for the Helmholtz operator with unknown $u = u(x, y)$ in the square $\Omega \equiv (-1, 1)^2$,

$$(-\nabla^2 + \gamma)u = s(x, y), \qquad u_{|\partial\Omega} = a(\ell),$$

where γ is a non-negative constant, $s(x, y)$ is a known source term, and $a(\ell)$ is the boundary datum, ℓ being an arclength parameter along the entire boundary $\partial\Omega$. As demonstrated by Bernardi and Maday [2, pp. 13–14], in order that $a(\ell)$ could be the trace of a function belonging to the Sobolev space $H^1(\Omega)$ it must be continuous at the four corners. Therefore, denoting the Dirichlet data on the bottom and top sides by $a^{\mathrm{b}}(x)$ and $a^{\mathrm{t}}(x)$, $|x| \le 1$, and on the left and right sides by $a^{\mathrm{l}}(y)$ and $a^{\mathrm{r}}(y)$, $|y| \le 1$, these four functions must satisfy the following set of *compatibility conditions* at the corners:

$$\begin{cases} a^{\mathrm{t}}(-1) = a^{\mathrm{l}}(1), & a^{\mathrm{t}}(1) = a^{\mathrm{r}}(1), \\ a^{\mathrm{b}}(-1) = a^{\mathrm{l}}(-1), & a^{\mathrm{b}}(1) = a^{\mathrm{r}}(-1). \end{cases}$$

As a consequence, we are led to indicate the corner values of the Dirichlet condition as

$$\begin{cases} a^{\mathrm{tl}} \equiv a^{\mathrm{t}}(-1) = a^{\mathrm{l}}(1), & a^{\mathrm{tr}} \equiv a^{\mathrm{t}}(1) = a^{\mathrm{r}}(1), \\ a^{\mathrm{bl}} \equiv a^{\mathrm{b}}(-1) = a^{\mathrm{l}}(-1), & a^{\mathrm{br}} \equiv a^{\mathrm{b}}(1) = a^{\mathrm{r}}(-1). \end{cases}$$

The spatial discretization of the Helmholtz equation is done by means of the Galerkin projection method employing the Legendre basis $L_n^*(x)$, $n \ge 0$, defined in Section 2. The approximate solution u_N is expanded in the double series

$$u_N(x, y) = \sum_{i=0}^{I} L_i^*(x) \, u_{i,j} \, L_j^*(y) \, \overline{\sum_{j=0}^{J}}.$$

The symbol $\overline{\sum}$ is used to indicate a summation acting on the expression on the left, instead of on the right, as the usual $\sum$. This special symbol was introduced to be fully adherent with the matrix notation used in [4] and is particularly convenient in the derivation of the algorithms to be presented.

3.2. Discrete Lifting of the Dirichlet Data

The presence of the (four) compatibility conditions at the corners has a consequence on the process accounting for the nonhomogeneous Dirichlet condition by means of a lifting. This is clearly seen when the lifting is performed *analytically*, as done, for instance, in [21, Sect. 4.2]. In the present article we formulate the lifting in a fully discrete form based on the point values of the Dirichlet data to make the Helmholtz spectral solver applicable also to the solution of the biharmonic problem as an uncoupled system of two second order elliptic equations. In this case the trace of one of the two unknowns is defined only in the discrete sense within the algorithm. As a consequence, in the following we introduce a lifting which is characterized by the successive treatment of the Dirichlet values at the corners with respect to the other values prescribed at points internal to the four sides. In this way the complete separation of variables at the spectral level is achieved, in conformity with the direct product nature of the polynomial approximation.

The lifting of the Dirichlet boundary datum $a(\ell)$ consists in expressing the solution u_N in two parts, as

$$u_N(x, y) = u_N^0(x, y) + u_N^a(x, y),$$

where $u_N^0(x, y)$ satisfies the homogeneous Dirichlet condition, whereas $u_N^a(x, y)$ is an arbitrary function which approximates $a(\ell)$ on $\partial\Omega$.

To determine the lifting $u_N^a(x, y)$ we choose to split it in two separate contributions,

$$u_N^a(x, y) = u_N^{a,\mathrm{c}}(x, y) + u_N^{a,\mathrm{s}}(x, y),$$

where $u_N^{a,\mathrm{c}}(x, y)$ is the component to account for nonzero Dirichlet values at the *corners* while $u_N^{a,\mathrm{s}}(x, y)$ is the component to relieve the nonzero boundary values in the interior of the *sides*.

The first component $u_N^{a,\mathrm{c}}(x, y)$ is determined by a collocative approach, which enables one to satisfy the Dirichlet boundary condition in a strong sense exclusively at the corners. This is indeed a useful property, especially if one considers the method as a starting point for applications to more complex domains via a domain decomposition approach. The second component $u_N^{a,\mathrm{s}}(x, y)$ of the lifting is defined by the Galerkin–Legendre approach, which guarantees the optimality of the approximation (in L^2 norm). The combination of these two components is finally used to perturb the right hand side of the discrete Helmholtz equation to obtain the final system of algebraic equations.

It is convenient to introduce the following partitioning of a matrix of Legendre coefficients,

$$U = \left(\begin{array}{c|c} U^{(\mathrm{c})} & U^{(\mathrm{v})} \\ \hline U^{(\mathrm{h})} & U^{(\mathrm{i})} \end{array}\right),$$

where $U^{(\mathrm{c})}$ is the 2×2 matrix associated with the basis elements which are nonzero on the corners, $U^{(\mathrm{h})}$ and $U^{(\mathrm{v})}$ are $(I-1) \times 2$ and $2 \times (J-1)$ rectangular matrices associated with basis functions which are nonzero respectively on the horizontal and vertical sides, but for the interval extremes, and finally $U^{(\mathrm{i})}$ is a $(I-1) \times (J-1)$ matrix which contains the coefficients pertaining only to the "internal modes." According to this partitioning shown by the rectangle in Fig. 0, the matrix representation of the Legendre coefficients of the lifting $u_N^a(x, y)$ will be

$$U^a = \left(\begin{array}{c|c} U^{a\,(\mathrm{c})} & U^{a\,(\mathrm{v})} \\ \hline U^{a\,(\mathrm{h})} & 0 \end{array}\right).$$

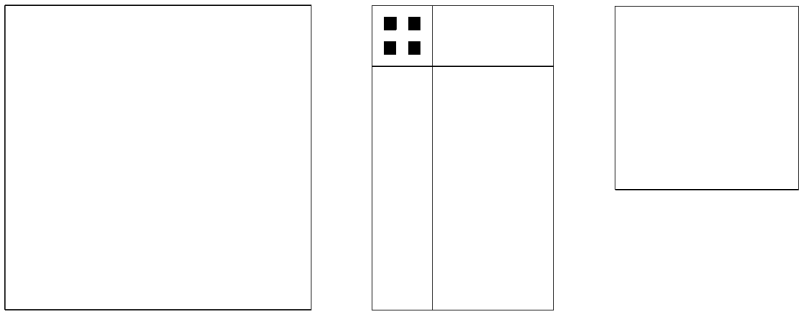

FIG. 0. Schematic of the matrix structure of the 2D Helmholtz problem discretized by the Galerkin–Legendre spectral method.

3.2.1. *Corner Component of the Lifting*

As anticipated, the corner component $u_N^{a,\mathrm{c}}(x, y)$ of the lifting is determined by a collocative approach, i.e., we write

$$\begin{cases} u^{a,\mathrm{c}}(-1, 1) = a^{\mathrm{tl}}, & u^{a,\mathrm{c}}(1, 1) = a^{\mathrm{tr}}, \\ u^{a,\mathrm{c}}(-1, -1) = a^{\mathrm{bl}}, & u^{a,\mathrm{c}}(1, -1) = a^{\mathrm{br}}. \end{cases}$$

It is natural to seek this part of the lifting in the subspace spanned by the basis functions of (x, y) which are nonzero on the corners, namely, $L_0^*(x)L_0^*(y)$, $L_0^*(x)L_1^*(y)$, $L_1^*(x)L_0^*(y)$, $L_1^*(x)L_1^*(y)$. Accordingly, using the direct-product notation, we have

$$u_N^{a,\mathrm{c}}(x, y) = \begin{pmatrix} L_0^*(x) & L_1^*(x) \end{pmatrix} U^{a\,(\mathrm{c})} \begin{pmatrix} L_0^*(y) \\ L_1^*(y) \end{pmatrix}.$$

Therefore the system of four equations can be written compactly as

$$\begin{pmatrix} L_0^*(-1) & L_1^*(-1) \\ L_0^*(1) & L_1^*(1) \end{pmatrix} U^{a\,(\mathrm{c})} \begin{pmatrix} L_0^*(-1) & L_0^*(1) \\ L_1^*(-1) & L_1^*(1) \end{pmatrix} = \begin{pmatrix} a^{\mathrm{bl}} & a^{\mathrm{tl}} \\ a^{\mathrm{br}} & a^{\mathrm{tr}} \end{pmatrix}$$

and is nonsingular.

3.2.2. *Side Component of the Lifting*

Once $U^{a\,(\mathrm{c})}$ has been determined, the second step of the lifting consists in evaluating its side component $u_N^{a,\mathrm{s}}(x, y)$, namely, to compute $U^{a\,(\mathrm{h})}$ and $U^{a\,(\mathrm{v})}$ by means of the (1D) Galerkin–Legendre approach. The function $u_N^{a,\mathrm{s}}(x, y)$ will be sought in the subspace spanned by basis functions of (x, y) that are zero on the corners and nonzero on the sides, and whose trace on the boundary is the orthogonal projection, in the sense of the L^2 inner-product, of the boundary datum once the corner nonhomogeneous part has been subtracted. In other terms, we have to determine $u_N^{a,\mathrm{s}}(x, y)$ such that

$$\oint_{\partial\Omega} v u_N^{a,\mathrm{s}} = \oint_{\partial\Omega} v\big(a - u_N^{a,\mathrm{c}}\big),$$

where $v(x, y)$ represents any function belonging to the same subspace in which $u_N^{a,\mathrm{s}}(x, y)$ is sought.

Writing the boundary integral as the sum of the contributions due to the four sides, the orthogonal projection can be written as

$$\begin{aligned} &\int_{\partial\Omega^{\mathrm{b}}} v u_N^{a,\mathrm{s}} + \int_{\partial\Omega^{\mathrm{t}}} v u_N^{a,\mathrm{s}} + \int_{\partial\Omega^{\mathrm{l}}} v u_N^{a,\mathrm{s}} + \int_{\partial\Omega^{\mathrm{r}}} v u_N^{a,\mathrm{s}} \\ &\quad = \int_{\partial\Omega^{\mathrm{b}}} v\big(a^{\mathrm{b}} - u_N^{a,\mathrm{c}}\big) + \int_{\partial\Omega^{\mathrm{t}}} v\big(a^{\mathrm{t}} - u_N^{a,\mathrm{c}}\big) + \int_{\partial\Omega^{\mathrm{l}}} v\big(a^{\mathrm{l}} - u_N^{a,\mathrm{c}}\big) + \int_{\partial\Omega^{\mathrm{r}}} v\big(a^{\mathrm{r}} - u_N^{a,\mathrm{c}}\big). \end{aligned}$$

By virtue of the vanishing of any v at the corners, the contributions of the top and bottom sides can be uncoupled from those deriving from the left and right sides by choosing test functions which are nonzero on the horizontal sides and vanish on the vertical ones, and

vice versa, and by expanding the lifting in the same basis. Eventually, the whole problem separates in two independent ones, each of them being associated with two parallel sides:

$$\int_{\partial\Omega^{\mathrm{b}}} v u_N^{a,\mathrm{s}} + \int_{\partial\Omega^{\mathrm{t}}} v u_N^{a,\mathrm{s}} = \int_{\partial\Omega^{\mathrm{b}}} v\big(a^{\mathrm{b}} - u_N^{a,\mathrm{c}}\big) + \int_{\partial\Omega^{\mathrm{t}}} v\big(a^{\mathrm{t}} - u_N^{a,\mathrm{c}}\big),$$

$$\int_{\partial\Omega^{\mathrm{l}}} v u_N^{a,\mathrm{s}} + \int_{\partial\Omega^{\mathrm{r}}} v u_N^{a,\mathrm{s}} = \int_{\partial\Omega^{\mathrm{l}}} v\big(a^{\mathrm{l}} - u_N^{a,\mathrm{c}}\big) + \int_{\partial\Omega^{\mathrm{r}}} v\big(a^{\mathrm{r}} - u_N^{a,\mathrm{c}}\big).$$

Let us express each of the two problems in a discrete form and consider first the problem associated with the horizontal sides. We introduce the test functions

$$L_i^*(x)L_j^*(y), \qquad \text{for } 2 \le i \le I \text{ and } j = 0, 1,$$

and the expansion

$$u_N^{a,\mathrm{s}}(x,y) = \sum_{i=2}^{I} L_i^*(x) U^{a\,(\mathrm{h})} L_j^*(y) \sum_{j=0,1} + \sum_{i=0,1} L_i^*(x) U^{a\,(\mathrm{v})} L_j^*(y) \sum_{j=2}^{J}.$$

Now, by taking $v(x,y) = L_{i'}^*(x)L_{j'}^*(y)$ with $2 \le i' \le I$ and $j' = 0, 1$, the discrete form of the problem becomes, after interchanging integration and summation,

$$\begin{aligned}
&\sum_{i=2}^{I}\left(\int_{-1}^{1} L_{i'}^*(x)L_i^*(x)\,dx\right) U_{i,j}^{a\,(\mathrm{h})} L_j^*(-1) \sum_{j=0,1} L_{j'}^*(-1) \\
&\quad + \sum_{i=2}^{I}\left(\int_{-1}^{1} L_{i'}^*(x)L_i^*(x)\,dx\right) U_{i,j}^{a\,(\mathrm{h})} L_j^*(1) \sum_{j=0,1} L_{j'}^*(1) \\
&= \int_{-1}^{1} L_{i'}^*(x) a^{\mathrm{b}}(x)\,dx\, L_{j'}^*(-1) \;+\; \int_{-1}^{1} L_{i'}^*(x) a^{\mathrm{t}}(x)\,dx\, L_{j'}^*(1) \\
&\quad - \sum_{i=0,1}\left(\int_{-1}^{1} L_{i'}^*(x)L_i^*(x)\,dx\right) U_{i,j}^{a\,(\mathrm{c})} L_j^*(-1) \sum_{j=0,1} L_{j'}^*(-1) \\
&\quad - \sum_{i=0,1}\left(\int_{-1}^{1} L_{i'}^*(x)L_i^*(x)\,dx\right) U_{i,j}^{a\,(\mathrm{c})} L_j^*(1) \sum_{j=0,1} L_{j'}^*(1).
\end{aligned}$$

In terms of the mass matrix elements $M_{i',i} = \int_{-1}^{1} L_{i'}^*(x)L_i^*(x)\,dx$, the equation above can be written compactly as

$$\begin{aligned}
&\sum_{i=2}^{I} M_{i',i} U_{i,j}^{a\,(\mathrm{h})} \big[L_j^*(-1)L_{j'}^*(-1) + L_j^*(1)L_{j'}^*(1)\big] \sum_{j=0,1} \\
&\quad = \int_{-1}^{1} L_{i'}^*(x) a^{\mathrm{b}}(x)\,dx\, L_{j'}^*(-1) + \int_{-1}^{1} L_{i'}^*(x) a^{\mathrm{t}}(x)\,dx\, L_{j'}^*(1) \\
&\qquad - \sum_{i=0,1} M_{i',i} U_{i,j}^{a\,(\mathrm{c})} \big[L_j^*(-1)L_{j'}^*(-1) + L_j^*(1)L_{j'}^*(1)\big] \sum_{j=0,1}.
\end{aligned}$$

Introducing the 2×2 matrix H with elements $H_{i,j} = L_i^*(-1)L_j^*(-1) + L_i^*(1)L_j^*(1)$, $i = 0, 1$,

and $j = 0, 1$, the weak equations become, for every $2 \le i' \le I$ and $j' = 0, 1$,

$$\sum_{i=2}^{I} M_{i',i} U_{i,j}^{a\,(\mathrm{h})} H_{j,j'} \sum_{j=0,1} = \int_{-1}^{1} L_{i'}^{*}(x) a^{\mathrm{b}}(x)\, dx\, L_{j'}^{*}(-1) + \int_{-1}^{1} L_{i'}^{*}(x) a^{\mathrm{t}}(x)\, dx\, L_{j'}^{*}(1) - \sum_{i=0,1} M_{i',i} U_{i,j}^{a\,(\mathrm{c})} H_{j,j'} \sum_{j=0,1}.$$

In the actual algorithm, the integrals on the right-hand side are evaluated approximately by means of the Gauss–Legendre quadrature formula to give, for instance,

$$\int_{-1}^{1} L_{i'}^{*}(x)\, a^{\mathrm{b}}(x)\, dx = \sum_{g=1}^{I+1} L_{i'}^{*}(x_g)\, w_g a^{\mathrm{b}}(x_g),$$

where x_g and w_g, $1 \le g \le I+1$, are the quadrature nodes and their respective weights. Accordingly, the previous weak equations assume the form

$$\sum_{i=2}^{I} M_{i',i} U_{i,j}^{a\,(\mathrm{h})} H_{j,j'} \sum_{j=0,1} = \sum_{g=1}^{I+1} L_{i'}^{*}(x_g) w_g \left[a^{\mathrm{b}}(x_g) L_{j'}^{*}(-1) + a^{\mathrm{t}}(x_g) L_{j'}^{*}(1) \right] - \sum_{i=0,1} M_{i',i} U_{i,j}^{a\,(\mathrm{c})} H_{j,j'} \sum_{j=0,1}.$$

The whole system can be recast in matrix form by introducing the vector of the Gauss–Legendre weights

$$\mathcal{W} \equiv \{w_g, 1 \le g \le I+1\},$$

the array $\mathcal{L}$ of values of the Legendre functions computed at the Gauss–Legendre nodes,[1] namely,

$$\mathcal{L} \equiv \{\mathcal{L}_{g,i} = L_i^{*}(x_g), 1 \le g \le I+1, 0 \le i \le I\},$$

and finally the two vectors of the values of the Dirichlet conditions $a^{\mathrm{t}}(x)$ and $a^{\mathrm{b}}(x)$ at the same quadrature points:

$$\mathcal{A}^{\mathrm{t}} \equiv \left\{a^{\mathrm{t}}(x_g), 1 \le g \le I+1\right\},$$
$$\mathcal{A}^{\mathrm{b}} \equiv \left\{a^{\mathrm{b}}(x_g), 1 \le g \le I+1\right\}.$$

The full system in matrix form reads as

$$\boldsymbol{M} U_{*,0}^{a\,(\mathrm{h})} H = \mathcal{L}_{*,i}^{T} \left\{ \mathcal{W} \star \left[\mathcal{A}^{\mathrm{b}} \begin{pmatrix} L_0^{*}(-1) & L_1^{*}(-1) \end{pmatrix} + \mathcal{A}^{\mathrm{t}} \begin{pmatrix} L_0^{*}(1) & L_1^{*}(1) \end{pmatrix} \right] \right\} - M^{(\mathrm{h})} U^{a\,(\mathrm{c})} H,$$

where $\star$ denotes the element-by-element multiplication of vectors and where we introduced the following partitioning of the mass matrix,[2]

$$M = \begin{pmatrix} M^{(\mathrm{c})} & M^{(\mathrm{h})\,T} \\ M^{(\mathrm{h})} & \boldsymbol{M} \end{pmatrix}.$$

[1] Here and in the following, script letters are used to indicate quantities evaluated at Gauss–Legendre quadrature points.

[2] Sans serif characters are used throughout to denote vectors and matrices which pertain only to internal modes, that is, to basis functions vanishing at the extremes of the interval.

In particular, for our basis, the matrix H is diagonal and therefore the system of equations can be written as two fully decoupled systems each of $(I+1)$ unknowns. In fact, for the Legendre basis $L_i^*(x)$ one has

$$H = \begin{pmatrix} 2 & 0 \\ 0 & 1 \end{pmatrix},$$

and the two uncoupled systems to perform the lifting on the horizontal sides are

$$\boldsymbol{M} U_{*,0}^{a\,(\mathrm{h})} = \frac{1}{2}\mathcal{L}^T[\mathcal{W} \star (\mathcal{A}^{\mathrm{b}} + \mathcal{A}^{\mathrm{t}})] - M^{(\mathrm{h})} U_{*,0}^{a\,(\mathrm{c})},$$

$$\boldsymbol{M} U_{*,1}^{a\,(\mathrm{h})} = \frac{1}{\sqrt{2}}\mathcal{L}^T[\mathcal{W} \star (\mathcal{A}^{\mathrm{t}} - \mathcal{A}^{\mathrm{b}})] - M^{(\mathrm{h})} U_{*,1}^{a\,(\mathrm{c})}.$$

It is important to remark that, irrespective of such a decoupling, the side component of the lifting cannot be evaluated on a side by side base.

The same procedure can be adopted for the two vertical sides, and it is not repeated for conciseness; the result is the transpose of the former expression by virtue of the direct product nature of the basis and reads

$$U_{0,*}^{a\,(\mathrm{v})} \boldsymbol{N} = \frac{1}{2}[(\mathcal{A}^{\mathrm{l}} + \mathcal{A}^{\mathrm{r}})^T \star \mathcal{V}]\mathcal{K} - U_{0,*}^{a\,(\mathrm{c})} N^{(\mathrm{v})},$$

$$U_{1,*}^{a\,(\mathrm{v})} \boldsymbol{N} = \frac{1}{\sqrt{2}}[(\mathcal{A}^{\mathrm{r}} - \mathcal{A}^{\mathrm{l}})^T \star \mathcal{V}]\mathcal{K} - U_{1,*}^{a\,(\mathrm{c})} N^{(\mathrm{v})},$$

where $\boldsymbol{N}$ is the counterpart for the y direction of the mass matrix $\boldsymbol{M}$, namely,

$$N = \begin{pmatrix} N^{(\mathrm{c})} & N^{(\mathrm{v})} \\ N^{(\mathrm{v})\,T} & \boldsymbol{N} \end{pmatrix},$$

the vector $\mathcal{V} \equiv \{w(x_g),\, 1 \le g \le J+1\}$ contains the weights of the Gauss–Legendre quadrature formula with $J+1$ nodes and $\mathcal{K} \equiv \{\mathcal{L}_{g,i} = L_i^*(x_g),\, 1 \le g \le J+1,\, 0 \le i \le J\}$. Therefore, the side component of the lifting requires us to solve two mass matrix problems of size $(I-1)$ and two problems of size $(J-1)$.

By summarizing, the set of boundary values which are needed by our spectral solution algorithm for the Dirichlet problem comprises the values prescribed on the unknown at the four corners as well as the values at the (1D) Gauss–Legendre points located on each side. Consequently, the proposed elliptic solver is fed by the following two sets of Dirichlet data,

$$\begin{cases} a^{\mathrm{tl}},\ a^{\mathrm{tr}}, \\ a^{\mathrm{bl}},\ a^{\mathrm{br}}, \end{cases} \quad \text{and} \quad \begin{cases} \{a^{\mathrm{t}}(x_g), a^{\mathrm{b}}(x_g),\, 1 \le g \le I+1\}, \\ \{a^{\mathrm{l}}(y_g), a^{\mathrm{r}}(y_g),\, 1 \le g \le J+1\}, \end{cases}$$

which amount to a total of $4 + 2(I+J+2) = 2(I+J) + 8$ distinct boundary values.

By contrast, spectral elliptic solvers based on the collocation method use a total of only $2(I+1) + 2(J-1) = 2(I+J)$ Dirichlet data [16]. Therefore the proposed method samples the Dirichlet boundary data at 8 more points than collocation schemes with the same number of polynomials. We feel that this treatment of the discrete Dirichlet data by our algorithm is essential for making it possible to determine the vorticity boundary value, including the corners, in the unregularized driven cavity problem by an uncoupled spectral method, since the wall distribution of vorticity is discontinuous (actually singularly discontinuous) at the two corners of the moving side of the cavity. It is worth concluding the presentation

of the discrete lifting for the two-dimensional problem by remarking that its extension to the three-dimensional elliptic equation with fully nonperiodic boundary conditions is not obvious unless one clarifies the nature of possible compatibility conditions for the Dirichlet data of the three-dimensional problem.

3.2.3. *Perturbation of the Right-Hand Side*

The lifting of the Dirichlet datum can be seen as a perturbation on the right-hand side of the linear system of the discretized version of the Helmholtz equation. In fact, by allowing all degrees of freedom including also those which are nonzero on $\partial\Omega$, the weak formulation of the Helmholtz equation reads

$$^0DUN + MU\,^0E + \gamma MUN = S,$$

where $U = U^0 + U^a$, ^0E is the y-counterpart of matrix ^0D, and S represents the Galerkin projection of the source $s(x, y)$ onto the Legendre basis, namely, $s_{i,j} = ((L_i^*(x)L_j^*(y), s(x, y)))$, $0 \le (i, j) \le (I, J)$, the integral being evaluated numerically by means of the direct-product Gauss–Legendre quadrature formula.

By exploiting the matrix partitionings introduced before, the system of equations pertaining to the internal test functions assumes the form

$$\begin{aligned}&\begin{pmatrix} D^{(\mathrm{h})} & \boldsymbol{D} \end{pmatrix} \begin{pmatrix} U^{a\,(\mathrm{c})} & U^{a\,(\mathrm{v})} \\ U^{a\,(\mathrm{h})} & \boldsymbol{U} \end{pmatrix} \begin{pmatrix} N^{(\mathrm{v})} \\ \boldsymbol{N} \end{pmatrix} + \begin{pmatrix} M^{(\mathrm{h})} & \boldsymbol{M} \end{pmatrix} \begin{pmatrix} U^{a\,(\mathrm{c})} & U^{a\,(\mathrm{v})} \\ U^{a\,(\mathrm{h})} & \boldsymbol{U} \end{pmatrix} \begin{pmatrix} E^{(\mathrm{v})} \\ \boldsymbol{E} \end{pmatrix} \\ &\quad + \gamma \begin{pmatrix} M^{(\mathrm{h})} & \boldsymbol{M} \end{pmatrix} \begin{pmatrix} U^{a\,(\mathrm{c})} & U^{a\,(\mathrm{v})} \\ U^{a\,(\mathrm{h})} & \boldsymbol{U} \end{pmatrix} \begin{pmatrix} N^{(\mathrm{v})} \\ \boldsymbol{N} \end{pmatrix} = \boldsymbol{S},\end{aligned}$$

where $\boldsymbol{U} = U^{0,\,(\mathrm{i})}$ and $\boldsymbol{S} = S^{(\mathrm{i})}$. Since the coefficients in $U^{(\mathrm{c})}$, $U^{(\mathrm{h})}$, and $U^{(\mathrm{v})}$ are known, the relation above can be rewritten transferring the corresponding terms to the right-hand side. In particular, for the Legendre basis we are working with, submatrices $D^{(\mathrm{h})}$ and $E^{(\mathrm{v})}$ are null and the right-hand side becomes

$$\boldsymbol{S} \;\rightarrow\; \boldsymbol{R} = \boldsymbol{S} - \boldsymbol{A},$$

where

$$\begin{aligned}\boldsymbol{A} = \boldsymbol{A}[a, \gamma] = {} & \boldsymbol{D}U^{a\,(\mathrm{h})}N^{(\mathrm{v})} + M^{(\mathrm{h})}U^{a\,(\mathrm{v})}\boldsymbol{E} \\ & + \gamma\left(M^{(\mathrm{h})}U^{a\,(\mathrm{c})}N^{(\mathrm{v})} + M^{(\mathrm{h})}U^{a\,(\mathrm{v})}\boldsymbol{N} + \boldsymbol{M}U^{a\,(\mathrm{h})}N^{(\mathrm{v})}\right).\end{aligned}$$

Note that, when the source term of the Helmholtz equation is known in terms of its Legendre coefficients S, instead of its L^2 projection, the right-hand side of the discrete system above assumes the form

$$\boldsymbol{R} = \overline{\overline{MSN}} - \boldsymbol{A},$$

where the double bar denotes the suppression of both the first two columns and the first two rows of the underlying matrix.

3.3. Mass-Matrix-Based Bidiagonalization Algorithm

The final system of discrete equations to be solved assumes the form

$$\boldsymbol{DUN} + \boldsymbol{MUE} + \gamma\boldsymbol{MUN} = \boldsymbol{R},$$

where

$$\boldsymbol{D} = \boldsymbol{I}_{(I-1)}, \qquad \boldsymbol{E} = \boldsymbol{I}_{(J-1)},$$
$$\boldsymbol{U} = \{u_{i,j}, 2 \le (i, j) \le (I, J)\},$$
$$\boldsymbol{M} = \{m_{i,i'} = (L_i^*(x), L_{i'}^*(x)), 2 \le (i, i') \le I\},$$
$$\boldsymbol{N} = \{n_{j,j'} = (L_j^*(y), L_{j'}^*(y)), 2 \le (j, j') \le J\}.$$

We retain the identity matrices $\boldsymbol{D}$ and $\boldsymbol{E}$ in the expression above to emphasize that for a *rectangular* domain suitable scaling coefficients must be included.

To solve this linear system, in a preliminary step we solve the symmetric eigenvalue problem [1] for the two mass matrices $\boldsymbol{M}$ and $\boldsymbol{N}$, namely, $\boldsymbol{M}\boldsymbol{w}^{(i)} = \lambda_i \boldsymbol{w}^{(i)}$, $2 \le i \le I$, $\boldsymbol{W} \equiv [\boldsymbol{w}^{(2)}, \ldots, \boldsymbol{w}^{(I)}]$, and $\boldsymbol{N}\boldsymbol{v}^{(j)} = \sigma_j \boldsymbol{v}^{(j)}$, $2 \le j \le J$, $\boldsymbol{V} \equiv [\boldsymbol{v}^{(2)}, \ldots, \boldsymbol{v}^{(J)}]$, so that $\boldsymbol{W}^T\boldsymbol{M}\boldsymbol{W} = \boldsymbol{\Lambda}$ and $\boldsymbol{V}^T\boldsymbol{N}\boldsymbol{V} = \boldsymbol{\Sigma}$, where $\boldsymbol{\Lambda}$ and $\boldsymbol{\Sigma}$ denote the diagonal matrices of the eigenvalues of $\boldsymbol{M}$ and $\boldsymbol{N}$, respectively.

As a consequence of the double transformation $\boldsymbol{R} \to \tilde{\boldsymbol{R}} = \boldsymbol{W}^T\boldsymbol{R}\boldsymbol{V}$ and the analogous one for $\boldsymbol{U}$, the linear system becomes

$$\boldsymbol{U}\boldsymbol{\Sigma} + \boldsymbol{\Lambda}\boldsymbol{U} + \gamma\boldsymbol{\Lambda}\boldsymbol{U}\boldsymbol{\Sigma} = \tilde{\boldsymbol{R}},$$

which is solved, componentwise, by

$$u_{i,j} = r_{i,j}/(\sigma_j + \lambda_i + \gamma\lambda_i\sigma_j), \qquad 2 \le (i, j) \le (I, J).$$

The sought for solution is then obtained by computing the anti-transform $\boldsymbol{U} \to \boldsymbol{U} = \boldsymbol{W}\boldsymbol{U}\boldsymbol{V}^T$ and finally merging $\boldsymbol{U}$ with the precomputed Legendre coefficients of the lifting, to give

$$U = \begin{pmatrix} U^{a\,(\mathrm{c})} & U^{a\,(\mathrm{v})} \\ U^{a\,(\mathrm{h})} & \boldsymbol{U} \end{pmatrix}.$$

3.4. Numerical Tests

The algorithm has been tested first by solving the Poisson equation supplemented by the homogeneous Dirichlet condition with the exact solution $u = \sin(4\pi x)\sin(4\pi y)$ considered in [12]. The maximum pointwise errors of the proposed Galerkin–Legendre algorithm are compared in Table I with the results provided by the *tau*-Chebyshev method [12] and the Galerkin–Legendre method of Shen [12]. The present method is always more accurate than its *tau*-Chebyshev counterpart but does not reach the accuracy of the (single) diagonalization method of Shen.

TABLE I
Maximum Pointwise Error: Solution $u = \sin(4\pi x)\sin(4\pi y)$

$I \times J$	*tau*-Cheb. [12]	Gal.–Leg. [21]	Gal.–Leg.
16×16	3.33×10^{-2}	2.93×10^{-3}	2.82×10^{-2}
32×32	4.77×10^{-11}	3.44×10^{-13}	2.55×10^{-11}
64×64	8.67×10^{-13}	5.55×10^{-15}	4.10×10^{-15}
128×128	2.00×10^{-12}	6.88×10^{-15}	5.44×10^{-15}

TABLE II
Maximum Pointwise Error: Solution $u = x^2 + e^{2x+y}$

$I \times J$	Galerkin–Legendre
8×8	2.32×10^{-5}
16×16	4.44×10^{-13}
32×32	1.04×10^{-12}

The second example is the solution of the Helmholtz equation with $\gamma = 1.5$ supplemented by the nonhomogeneous boundary condition, the exact solution being $u = x^2 + e^{2x+y}$. The numerical errors for different resolutions are given in Table II.

4. VORTICITY AND STREAM FUNCTION EQUATIONS

4.1. Uncoupled Formulation

Let us consider the Navier–Stokes equations for 2D flows expressed in terms of the variables vorticity ζ and stream function ψ. Taking into account the nonlinear advection term explicitly, the equations discretized in time can be written in the following uncoupled form [18]

$$(-\nabla^2 + \gamma)\zeta = f, \qquad \int_\Omega \eta\zeta = \oint_{\partial\Omega} \left(\frac{\partial \eta}{\partial n} a - \eta b \right),$$
$$-\nabla^2 \psi = \zeta, \qquad \psi_{|\partial\Omega} = a,$$

where $\gamma = \mathrm{Re}/\Delta t$, $f = \gamma \zeta^{\mathrm{old}} - \mathrm{Re}\, J(\zeta^{\mathrm{old}}, \psi^{\mathrm{old}})$, $\zeta = \zeta^{\mathrm{new}}$, and $\psi = \psi^{\mathrm{new}}$. In the integral conditions above, η represents any function harmonic in the computational domain Ω, while a and b denote the boundary data for ψ and $(\partial\psi/\partial n)$, respectively, which can be expressed in terms of the velocity specified on the boundary $\partial\Omega$. As previously stated, the Dirichlet datum a must be assumed to be continuous at the four corners [2, p. 93], while the Neumann datum b is *not* required to satisfy such a condition [and in fact b is discontinuous in the classical (*i.e.*, not regularized) driven cavity problem, to be considered in the numerical tests]. For an iterative multigrid method for the spectral solution of the coupled system of ζ-ψ equations the reader is referred to [13].

4.2. Spectral Influence Matrix

To enforce the vorticity integral conditions one introduces the decomposition of ζ

$$\zeta = \zeta^0 + \sum_{k'=1}^{\infty} \lambda_{k'} \zeta^{k'},$$

where ζ^0 and $\zeta^{k'}$ are the solution of auxiliary Dirichlet problems for the operator $(-\nabla^2 + \gamma)$ with suitable boundary conditions. In particular the traces of the functions $\zeta^{k'}$ constitute a basis for the Sobolev space $H^{1/2}(\partial\Omega)$. The imposition of the integral conditions gives the

linear problem for the unknowns $\lambda_{k'}$, $k' = 1, 2, \ldots$,

$$A\lambda = \beta,$$

where

$$A_{k,k'} = \int_\Omega \eta^k \zeta^{k'}, \qquad k, k' = 1, 2, \ldots$$
$$\beta_k = -\int_\Omega \eta^k \zeta^0 - \oint_{\partial\Omega} \eta^k b, \qquad k = 1, 2, \ldots.$$

By adopting the Glowinski–Pironneau method (for details see [18]), one can get rid of the harmonic functions η^k by introducing auxiliary functions w^k at the expense of solving one additional elliptic equation for each $k = 1, 2, \ldots$. The w^k's are such that their trace is coincident with that of the harmonic functions while, for the rest, they are completely arbitrary. In terms of these functions, the influence operator A and the right-hand side β can be shown to be characterized equivalently by

$$A_{k,k'} = \int_\Omega \left(w^k \zeta^{k'} - \boldsymbol{\nabla} w^k \cdot \boldsymbol{\nabla} \psi^{k'}\right),$$
$$\beta_k = -\int_\Omega \left(w^k \zeta^0 - \boldsymbol{\nabla} w^k \cdot \boldsymbol{\nabla} \psi^0\right) - \oint_{\partial\Omega} w^k b,$$

where the fields $\psi^{k'}$ and ψ^0 are solutions to additional Dirichlet problems for the Laplace operator [18].

Coming now to the problem discretized by the Legendre spectral method, we introduce the finite dimensional basis $\{w^k(x, y), 1 \le k \le 2(I + J)\}$ of functions defined as

$$\begin{cases} w^{1+i}(x, y) = L_i^*(x), & w^{I+2+i}(x, y) = L_i^*(x)\frac{y}{\sqrt{2}}, & 0 \le i \le I, \\ w^{2I+1+j}(x, y) = L_j^*(y), & w^{2I+J+j}(x, y) = \frac{x}{\sqrt{2}} L_j^*(y), & 2 \le j \le J. \end{cases}$$

Thus, the discrete basis consists of the four "groups" of functions above, that will be indicated by $w^{(1)}$, $w^{(2)}$, $\overline{w}^{(3)}$, and $\overline{w}^{(4)}$ in the following, where the overbar is used to emphasize that the components corresponding to $j = 0$ and $j = 1$ are excluded since they are already accounted for by the first two components of $w^{(1)}$ and $w^{(2)}$. In other words, the four functions w^k with nonzero value at the corners are included as the first two components of $w^{(1)}$ and $w^{(2)}$. This will cause a seemingly asymmetric treatment of the two directions x and y in some later expressions.

The discrete representation of the unknown fields ζ and ψ is

$$\zeta_N(x, y) = \sum_{i=0}^{I} L_i^*(x)\, \zeta_{i,j}\, L_j^*(y) \sum_{j=0}^{J},$$
$$\psi_N(x, y) = \sum_{i=0}^{I} L_i^*(x)\, \psi_{i,j}\, L_j^*(y) \sum_{j=0}^{J},$$

and we denote the Legendre coefficients collectively by matrices $Z = \{\zeta_{i,j}, 0 \le (i, j) \le (I, J)\}$ and $\Psi = \{\psi_{i,j}, 0 \le (i, j) \le (I, J)\}$.

The influence matrix A_N of order $2(I+J)$ is constructed and gives the symmetric definite positive linear system

$$A_N \boldsymbol{\lambda} = \boldsymbol{\beta},$$

with $\boldsymbol{\lambda} = \{\lambda_k, 1 \le k \le 2(I+J)\}$ and $\boldsymbol{\beta} = \{\beta_k, 1 \le k \le 2(I+J)\}$.

We consider now the k'th column vector of A_N, denoted by $\boldsymbol{\alpha}$, which involves the functions $\zeta_N^{k'}$ and $\psi_N^{k'}$, indicated here by ζ_N and ψ_N, for conciseness; we have

$$\alpha_k = \int_\Omega \left(w^k \zeta_N - \boldsymbol{\nabla} w^k \cdot \boldsymbol{\nabla} \psi_N \right), \qquad 1 \le k \le 2(I+J).$$

Let us consider the two contributions to the integral separately and denote them as

$$\gamma_k = \int_\Omega w^k \zeta_N \qquad \text{and} \qquad \delta_k = \int_\Omega \boldsymbol{\nabla} w^k \cdot \boldsymbol{\nabla} \psi_N.$$

A direct integration allows us to determine the four "segments" of the vector $\boldsymbol{\gamma}$ which correspond to the four subsets of basis functions w^k defined above:

$$\gamma^{(1)} = M Z n_0, \qquad \gamma^{(2)} = M Z n_1,$$
$$\bar{\gamma}^{(3)} = \overline{{}_0 m Z N}, \qquad \bar{\gamma}^{(4)} = \overline{{}_1 m Z N}.$$

Here n_0, n_1, ${}_0m$, and ${}_1m$ denote the first two column and row vectors of N and M; namely, we have defined

$$n_0 \equiv n_{*,0}, \qquad n_1 \equiv n_{*,1},$$
$${}_0m \equiv m_{0,*}, \qquad {}_1m \equiv m_{1,*}.$$

Furthermore, the overbar indicates that the first two components of the vector (of length $J+1$) under it are skipped, to obtain a vector of length $J-1$, as both $\bar{\gamma}^{(3)}$ and $\bar{\gamma}^{(4)}$ are. It is important to note that the multiplication of Z by n_0, n_1, ${}_0m$, and ${}_1m$ in the expressions above is actually a linear combination of only two (column or row) vectors, since only two components of vectors n_0, n_1, ${}_0m$, and ${}_1m$ are different from zero: we have in fact

$$Z n_0 = \zeta_{*,0}\, n_{0,0} + \zeta_{*,2}\, n_{2,0},$$
$$Z n_1 = \zeta_{*,1}\, n_{1,1} + \zeta_{*,3}\, n_{3,1},$$

and similarly for the other two terms. In the same spirit, we notice that also the product by the mass matrices M and N involves only three elements per each row, due to their sparsity.

Once the four "segments" of $\boldsymbol{\gamma}$ have been evaluated, they are combined to give the global vector according to

$$\boldsymbol{\gamma} = \left\{ \gamma^{(1)}, \gamma^{(2)}, \bar{\gamma}^{(3)}, \bar{\gamma}^{(4)} \right\}.$$

The evaluation of the second contribution $\delta_k = \int_\Omega \boldsymbol{\nabla} w^k \cdot \boldsymbol{\nabla} \psi_N$ proceeds in the same way and by direct integration one obtains

$$\delta^{(1)} = {}^0D \Psi n_0, \qquad \delta^{(2)} = {}^0D \Psi n_1 + M \psi_{*,1},$$
$$\bar{\delta}^{(3)} = \overline{{}_0 m \Psi {}^0E}, \qquad \bar{\delta}^{(4)} = \overline{\psi_{1,*} N} + \overline{{}_1 m \Psi {}^0E}.$$

Again, the overbar indicates suppression of the first two components of the underlying vector. The compound vector is

$$\boldsymbol{\delta} = \left\{\delta^{(1)}, \delta^{(2)}, \overline{\delta}^{(3)}, \overline{\delta}^{(4)}\right\},$$

and the final expression of each column vector of A_N is

$$\boldsymbol{\alpha} = \boldsymbol{\gamma} - \boldsymbol{\delta}.$$

After the solution $\boldsymbol{\lambda}$ has been determined, the values at the corners and at Gauss–Legendre points of the sides—the input to the Helmholtz spectral solver—are evaluated from the expression

$$\zeta_N^{\text{int}}(x, y) = \sum_{i=0}^{I} L_i^*(x)\left[\lambda_{1+i} + \lambda_{I+2+i}\frac{y}{\sqrt{2}}\right] + \left[\lambda_{2I+1+j} + \frac{x}{\sqrt{2}}\lambda_{2I+J+j}\right] L_j^*(y) \sum_{j=2}^{J}.$$

By summarizing, the Glowinski–Pironneau method avoids the explicit construction of the harmonic functions occurring in the vorticity integral conditions but requires us to solve a double number of Dirichlet problems to determine the influence matrix A_N and the right-hand side $\boldsymbol{\beta}$. This spectral version of the Glowinski–Pironneau method differs from its finite-element counterpart in that the integration extends here over the entire domain instead of being limited to the strip of elements in contact with the boundary. However, by virtue of the high sparsity of matrices associated with the Legendre polynomials combined with the direct product nature of the 2D spectral approximation, the full-volume integrals can be evaluated very fast, as just shown. All the Dirichlet problems for the Helmholtz and Poisson equations of the uncoupled method are solved by means of the bidiagonalization algorithm described in Subsection 3.3.

4.2.1. *Even–Odd Uncoupling*

The method just described for enforcing the vorticity integral conditions presents the drawback that the influence matrix A_N is considered as a single full matrix, whereas it has very many zero entries because the even and odd components of the trace in a rectangular domain are not coupled by the operator A. Therefore, for computational efficiency, it is convenient to exploit the even–odd uncoupled character of A_N by introducing four subspaces of the space $\{w^k(x, y)\}$, each subspace being chosen so as to account for, respectively, the even–even, odd–even, even–odd, and odd–odd component of the trace. In the construction of these bases we are faced again with the subtlety of accounting properly (and not twice) the effect of the modes associated with functions which are nonzero at the four corners. The most natural bases for the four aforementioned uncoupled components of the trace are

$$\begin{cases} w^n_{(\text{ee})}(x, y) = L^*_{i_{\text{e}}(n)}(x), \quad i_{\text{e}}(n) = 2(n-1), & n = 1, 2, \ldots, \lfloor (I+2)/2 \rfloor; \\ w^n_{(\text{ee})}(x, y) = L^*_{j_{\text{e}}(n)}(y), \quad j_{\text{e}}(n) = 2[n - \lfloor (I+2)/2 \rfloor], & n = \lfloor (I+2)/2 \rfloor + 1, \ldots, \lfloor (I+2)/2 \rfloor \\ & \quad + \lfloor J/2 \rfloor; \end{cases}$$

$$\begin{cases} w^n_{(\text{oe})}(x, y) = L^*_{i_{\text{o}}(n)}(x), \quad i_{\text{o}}(n) = 2n-1, & n = 1, 2, \ldots, \lfloor (I+1)/2 \rfloor; \\ w^n_{(\text{oe})}(x, y) = \frac{x}{\sqrt{2}} L^*_{j_{\text{e}}(n)}(y), \quad j_{\text{e}}(n) = 2[n - \lfloor (I+1)/2 \rfloor], & n = \lfloor (I+1)/2 \rfloor + 1, \ldots, \lfloor (I+1)/2 \rfloor \\ & \quad + \lfloor J/2 \rfloor; \end{cases}$$

$$\begin{cases} w^n_{(\mathrm{eo})}(x,y) = L^*_{i_{\mathrm{e}}(n)}(x)\frac{y}{\sqrt{2}}, \quad i_{\mathrm{e}}(n) = 2(n-1), & n = 1, 2, \ldots, \lfloor (I+2)/2 \rfloor; \\ w^n_{(\mathrm{eo})}(x,y) = L^*_{j_{\mathrm{o}}(n)}(y), \quad j_{\mathrm{o}}(n) = 2[n - \lfloor (I+2)/2 \rfloor] + 1, & n = \lfloor (I+2)/2 \rfloor + 1, \ldots, \lfloor (I+2)/2 \rfloor \\ & \quad + \lfloor (J-1)/2 \rfloor; \end{cases}$$

$$\begin{cases} w^n_{(\mathrm{oo})}(x,y) = L^*_{i_{\mathrm{o}}(n)}(x)\frac{y}{\sqrt{2}}, \quad i_{\mathrm{o}}(n) = 2n - 1, & n = 1, 2, \ldots, \lfloor (I+1)/2 \rfloor; \\ w^n_{(\mathrm{oo})}(x,y) = \frac{y}{\sqrt{2}} L^*_{j_{\mathrm{o}}(n)}(y), \quad j_{\mathrm{o}}(n) = 2[n - \lfloor (I+1)/2 \rfloor] + 1, & n = \lfloor (I+1)/2 \rfloor + 1, \ldots, \\ & \quad \lfloor (I+1)/2 \rfloor + \lfloor (J-1)/2 \rfloor. \end{cases}$$

The single influence matrix A_N of dimension $2(I+J)$ is therefore replaced by the following four symmetric positive-definite matrices, indicated here with their respective dimensions,

$$A_{(\mathrm{ee})}, \left\lfloor \frac{I+2}{2} \right\rfloor + \left\lfloor \frac{J}{2} \right\rfloor, \qquad A_{(\mathrm{eo})}, \left\lfloor \frac{I+2}{2} \right\rfloor + \left\lfloor \frac{J-1}{2} \right\rfloor,$$

$$A_{(\mathrm{oe})}, \left\lfloor \frac{I+1}{2} \right\rfloor + \left\lfloor \frac{J}{2} \right\rfloor, \qquad A_{(\mathrm{oo})}, \left\lfloor \frac{I+1}{2} \right\rfloor + \left\lfloor \frac{J-1}{2} \right\rfloor.$$

To assess the conditioning of the four symmetric influence matrices, their condition numbers, in the Euclidean norm,

$$\chi_2 = \|A\|_2 \|A^{-1}\|_2 = \frac{\lambda_{\max}(A)}{\lambda_{\min}(A)},$$

are reported as a function of the matrix dimension M in Fig. 1, for $\gamma = 10^3$. This shows that $\chi_2 \propto M^3$ consistently with the behaviour of the condition number for Legendre spectral approximation to second order elliptic operators.

4.3. Nonlinear Term

The nonlinear term $J(\zeta, \psi)$ is evaluated according to the pseudospectral technique introduced by Orszag. This means that one looks for the L^2 projection on the basis functions of the Jacobian determinant

$$J_N(x,y) = \frac{\partial(\zeta_N, \psi_N)}{\partial(x,y)},$$

where the superscript $^{\mathrm{old}}$ has been suppressed for simplicity. In this section, the symbol J used to indicate the Jacobian determinant is not to be confused with the upper extreme of the range of j; the correct meaning of J should however be clear from the context.

To determine the values $\{J_{i,j}\}$ of the projection, one first introduces point values of the unknown variables at points in the physical space, for instance,

$$\zeta_N(x,y) \leftrightarrow Z \to \mathcal{Z} = \{\zeta_N(x_g, y_h), 1 \le g \le I+1, 1 \le h \le J+1\},$$

where x_g and y_h denote the Gauss–Legendre integration points over the interval $[-1, 1]$. As in Section 3, script letters are used to indicate quantities evaluated at Gauss–Legendre quadrature points.

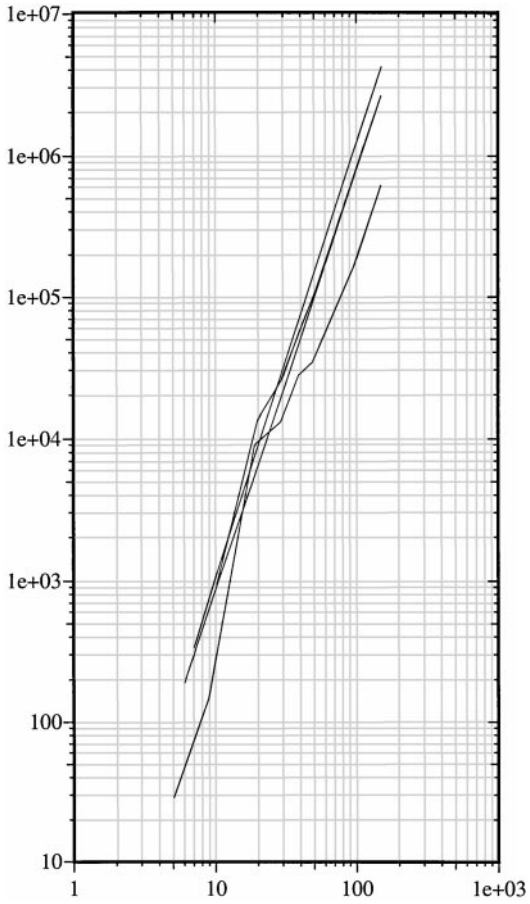

FIG. 1. Condition number of the four influence matrices for $\gamma = 1000$.

As a matter of fact, we need the values of the derivatives of $\zeta_N(x, y)$ and $\psi_N(x, y)$ at these points; for example, considering the derivative $\partial\zeta_N/\partial x$, its point values

$$\mathcal{Z}_{(x)} = \left\{ \left. \frac{\partial \zeta_N(x, y)}{\partial x} \right|_{x_g, y_h}, 1 \le g \le I + 1, 1 \le h \le J + 1 \right\}$$

are given by

$$\mathcal{Z}_{(x)} = \mathcal{L}' Z \mathcal{K}^T,$$

where we have introduced the point quantities

$$\mathcal{L} = \{\mathcal{L}_{g,i} = L_i^*(x_g), 1 \le g \le I + 1, 0 \le i \le I\},$$
$$\mathcal{L}' = \{\mathcal{L}'_{g,i} = L_i^*(x_g)', 1 \le g \le I + 1, 0 \le i \le I\},$$

and similarly for $\mathcal{K}$ and $\mathcal{K}'$, with the corresponding subscripts h and j ranging over $1 \le h \le J + 1$ and $0 \le j \le J$, respectively. Therefore, all the partial derivatives for the nonlinear

term are evaluated as

$$\mathcal{Z}_{(x)} = \mathcal{L}' Z \mathcal{K}^T, \qquad \mathcal{Z}_{(y)} = \mathcal{L} Z \mathcal{K}'^T,$$
$$\mathcal{P}_{(x)} = \mathcal{L}' \Psi \mathcal{K}^T, \qquad \mathcal{P}_{(y)} = \mathcal{L} \Psi \mathcal{K}'^T,$$

and the point values of the Jacobian determinant are obtained from the relation

$$\mathcal{J} = \mathcal{Z}_{(x)} \star \mathcal{P}_{(y)} - \mathcal{Z}_{(y)} \star \mathcal{P}_{(x)},$$

where $\star$ denotes the element-by-element multiplication of matrices.

As a consequence, the pseudospectral approximation of the nonlinear term is obtained by numerically projecting (in the L^2 sense) this term by means of the direct-product Gauss–Legendre quadrature formula with $(I+1) \times (J+1)$ points, to give

$$\int_{-1}^{1} \int_{-1}^{1} L_i^*(x) J_N(x, y) L_j^*(y)\, dx\, dy = \sum_{g=1}^{I+1} L_i^*(x_g) w_g \mathcal{J}_{g,h} v_h L_j^*(y_h) \sum_{h=1}^{J+1},$$

where w_g, $1 \le g \le I+1$, and v_h, $1 \le h \le J+1$, denote the weights of the 1D Gauss–Legendre formula with $(I+1)$ and $(J+1)$ points, respectively. The sought for matrix $J = \{J_{i,j}\}$ of the projection of the nonlinear term is given by

$$J = \mathcal{L}^T \mathcal{W} \mathcal{J} \mathcal{V} \mathcal{K},$$

where the Gauss–Legendre weights have been framed in the diagonal matrices

$$\mathcal{W} = \begin{pmatrix} w_1 & & & \\ & w_2 & & \\ & & \ddots & \\ & & & w_{I+1} \end{pmatrix} \quad \text{and} \quad \mathcal{V} = \begin{pmatrix} v_1 & & & \\ & v_2 & & \\ & & \ddots & \\ & & & v_{J+1} \end{pmatrix}.$$

Thus, the final right-hand side of the discrete vorticity equations reads

$$\boldsymbol{R} = \gamma \overline{\overline{M Z^{\text{old}} N}} - \text{Re}\, \boldsymbol{J}^{\text{old}},$$

to which the lifting of the vorticity boundary values has to be subtracted to give, actually,

$$\boldsymbol{R} = \gamma \overline{\overline{M Z^{\text{old}} N}} - \text{Re}\, \boldsymbol{J}^{\text{old}} - \boldsymbol{\Lambda},$$

where $\boldsymbol{\Lambda} = \boldsymbol{\Lambda}[\boldsymbol{\lambda}, \gamma]$.

4.4. Numerical Tests

We have applied the uncoupled algorithm to the solution of the driven cavity problem, *without* regularizing the velocity boundary condition at the corners, where the horizontal wall slides on the stationary vertical walls. At these two points the no-slip datum b is discontinuous when passing from the vertical to the horizontal walls. As a consequence, the solution of the not regularized problem has a singular behaviour at these points for any Reynolds number; the structure of the singularity of the steady solution at these two points has been investigated by Gupta *et al.* [11].

We first solved the creeping flow problem (Re = 0) by the spectral method using $I = J = 200$ over the unit square $[0, 1]^2$. The plot of the vorticity contours and the streamlines are given in Figs. 2a and 2b. The solution agrees fairly well with the known reference solution, except for the vorticity in a very narrow layer on the vertical sides and in the bottom corners, where ζ_N is found to be perturbed by small spatial oscillations at the smallest scales of the spatial resolution. This is clear evidence of a Gibbs' phenomenon caused by the attempt to resolve the strong singularity of the solution at the two top corners by means of a polynomial

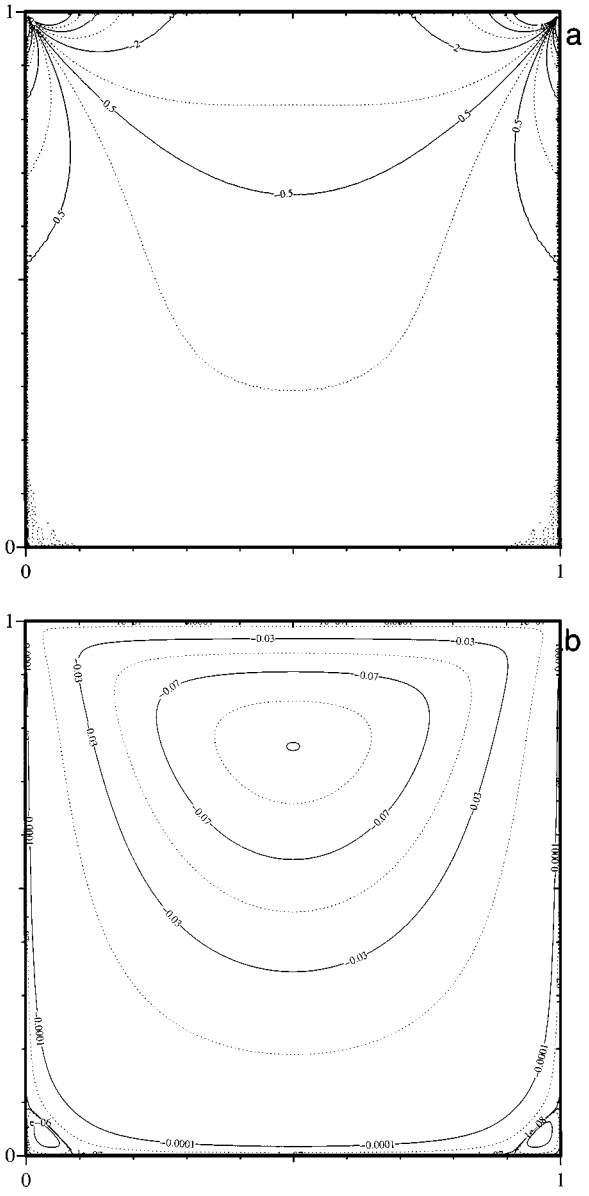

FIG. 2. Stokes flows in the square cavity problem, without regularization of the velocity boundary condition at the upper corners. Vorticity contours (a) and streamlines (b) for $I = J = 200$.

approximation with roots clustering near the interval extremes. The Stokes solution has been reported here just to emphasize that these Gibbs' oscillations are not related to the presence of nonlinear terms.

We notice that, in spite of this severe singularity, the present method provides a correct discrete solution which satisfies the global conservation law $\int_\Omega \zeta_N = -\oint_{\partial\Omega} b$—within round-off errors. This relation is in fact nothing but the integral condition with respect to the harmonic function $\eta(x, y) \equiv 1$.

One could observe that computing the vorticity field of the not regularized driven cavity problem by an uncoupled method is somewhat paradoxical. In fact, on the one hand the vorticity trace displays a very singular behaviour at the two upper corners, since $\zeta \to \infty$ or $-\infty$, according to whether the corner is approached along the vertical rather than the horizontal wall. On the other hand the boundary datum for solving the Dirichlet problem for ζ_N must be continuous at the corners. The point is that the proposed scheme employs the corner values as an independent meaningful component of the Dirichlet boundary data while, at the same time, it allows for a discontinuous behaviour near the corners, since the boundary values are specified at the Gauss–Legendre points of the four sides.

The second test calculation is the solution of the Navier–Stokes equations for $\mathrm{Re} = 1000$, starting form rest. The solution has been computed with $I = J = 100$ and $I = J = 150$, using a time step $\Delta t = 0.005$ and $\Delta t = 0.001$, respectively. The steady-state solutions ζ_N and ψ_N at $t = 50$ on the two grids are shown in Figs. 3 and 4 (maximal pointwise difference between the last two time steps 4.9×10^{-6} for ζ_N and 3.9×10^{-8} for ψ_N). The reduction of the spatial scale of Gibbs' oscillations as N $(=I = J)$ increases is evident. A comparison with the reference solution [3] in the eye-ball norm (which is surely adequate for the purpose of the present article) indicates that the computed spectral solutions are in a very satisfactory agreement, but for Gibbs' phenomenon, including fine features of the flow as the the two tertiary eddies in the bottom corners.

To check that Gibbs' spatial oscillations do not prevent the development of the correct dynamics, we report in Fig. 5 the unsteady solution at time $t = 6.25$, when the eddy generated at midheight on the downstream vertical side coalesces with the recirculation developing in the bottom right corner. The spectral solution for $I = J = 250$ is compared with another solution evaluated by means of a numerical scheme based on a new weak formulation of the ζ-ψ equations with an explicit treatment of the viscous diffusion term [10]. This formulation has been implemented by the finite element method using linear elements and adopting a second-order accurate BDF time discretization with a fully explicit account of the viscous and nonlinear terms *via* linear extrapolation in time. The mesh is nonuniform and consists of 2×80^2 triangles. The FEM solution depicted in Fig. 6 demonstrates that a correct simulation of transient flow is possible even in the presence of Gibbs' numerical pollution brought about by the corner singularities (the labels of the vorticity contours of the spectral and FEM solution are different due to different adimensionalizations).

We insist that the singular component of the steady solution was not subtracted in the present study purposely just to demonstrate that spectral solutions can be computed irrespective of the high singular behaviour of the vorticity field. The presence of spatial oscillations in ζ_N at the smallest wavelengths indicates that a proper treatment of the singularities is in order to recover spectral accuracy [3]. Alternatively, the problem could be modified by regularizing the boundary conditions as done, for instance, in the study about Hopf bifurcation in driven cavity flows by Shen [20].

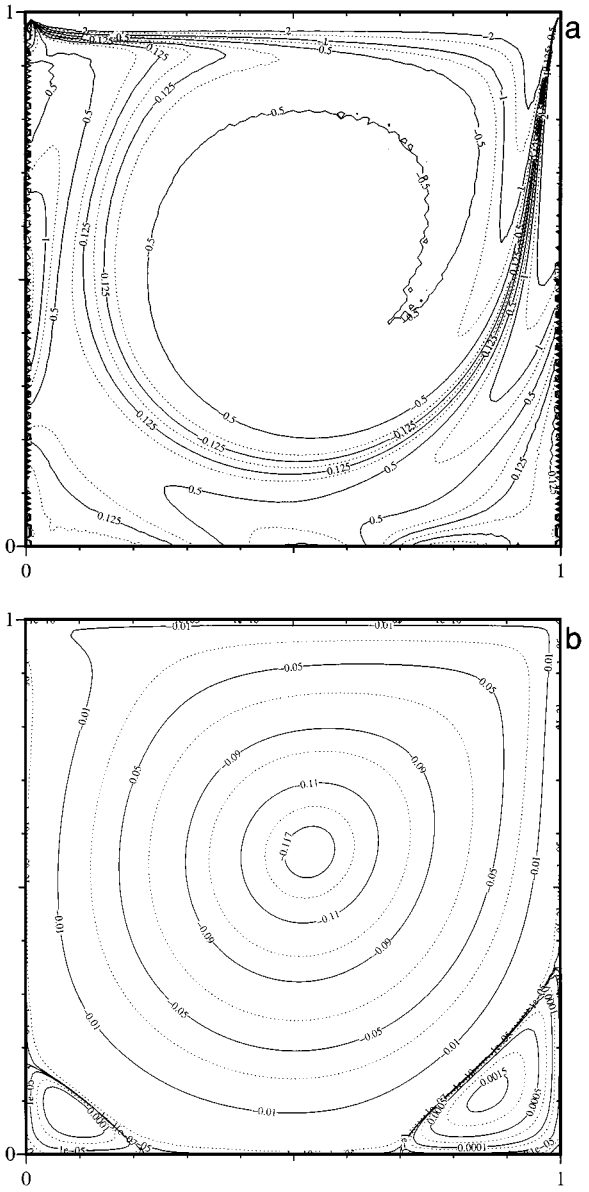

FIG. 3. Steady-state solution of the (unregularized) driven cavity problem for $\mathrm{Re} = 1000$. Vorticity contours (a) and streamlines (b) for $I = J = 100$.

5. CONCLUSIONS

We described a spectral method for solving the unsteady incompressible Navier–Stokes equations in a rectangular domain within no-slip boundaries, expressed in terms of the nonprimitive variables vorticity and stream function. An uncoupled formulation has been adopted by enforcing conditions of an integral type on the vorticity according to an adaptation of the Glowinski–Pironneau method to the present Galerkin–Legendre spatial discretization. The nonlinear term of the vorticity equation has been discretized in time in a fully explicit manner and has been evaluated according to the pseudospectral technique

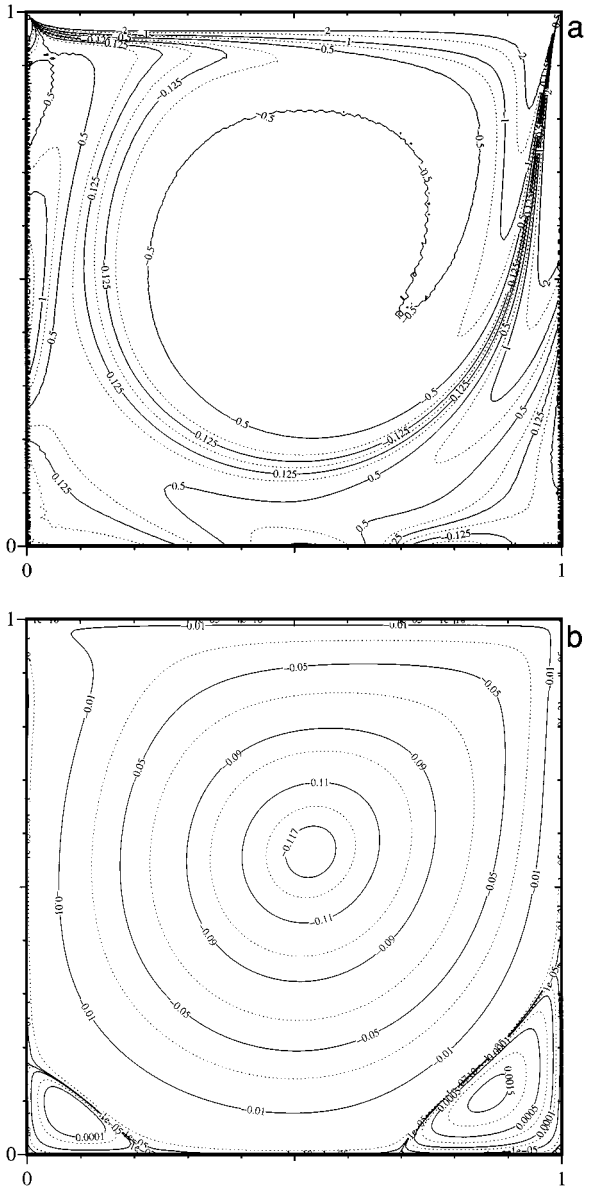

FIG. 4. Steady-state solution of the (unregularized) driven cavity problem for $\mathrm{Re} = 1000$. Vorticity contours (a) and streamlines (b) for $I = J = 150$.

of Orszag. The numerical scheme requires us to solve a cascade of elliptic equations, for building in a preprocessing phase the Glowinski–Pironneau influence matrix or the four smaller influence matrices associated with the uncoupled even/odd components of the unknown trace of vorticity. Then, each time step requires us to solve two pairs of Helmholtz and Poisson equations, both supplemented by Dirichlet boundary conditions, plus the single symmetric positive-definite linear system or the four irreducible independent systems of the same kind to enforce the vorticity integral conditions on the rectangular domain.

The second-order elliptic equations are solved by means of a bidiagonalization algorithm, after the effect of the possibly nonhomogeneous Dirichlet condition has been taken into

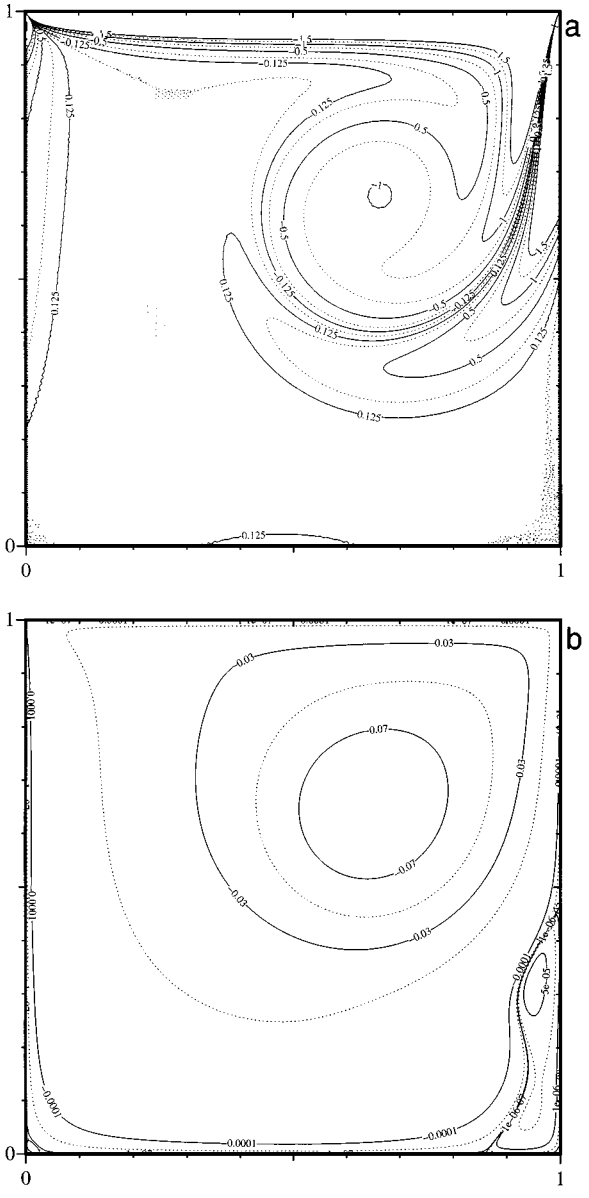

FIG. 5. Spectral solution of the unsteady (unregularized) driven cavity problem with impulsive start for $\mathrm{Re} = 1000$ at $t = 6.25$. Vorticity contours (a) and streamlines (b) for $I = J = 250$.

account by a lifting. The latter is formulated at the level of the discrete equations and in a form fully compatible with a direct product implementation of the algorithm. In this way, the proposed spectral method achieves the highest degree of separation of variables in the solution of the biharmonic problem as a system of split equations which is compatible with the presence of nonperiodic boundary conditions in both spatial directions. Under these hypotheses, a complete variable separation of the spatial dependence in the two directions is possible for each of the component Poisson equations, but, at the same time, a nonseparable aspect remains in the uncoupled solution algorithm as a consequence of the fact that the four influence matrix operators "go all around" the entire boundary of the computational domain.

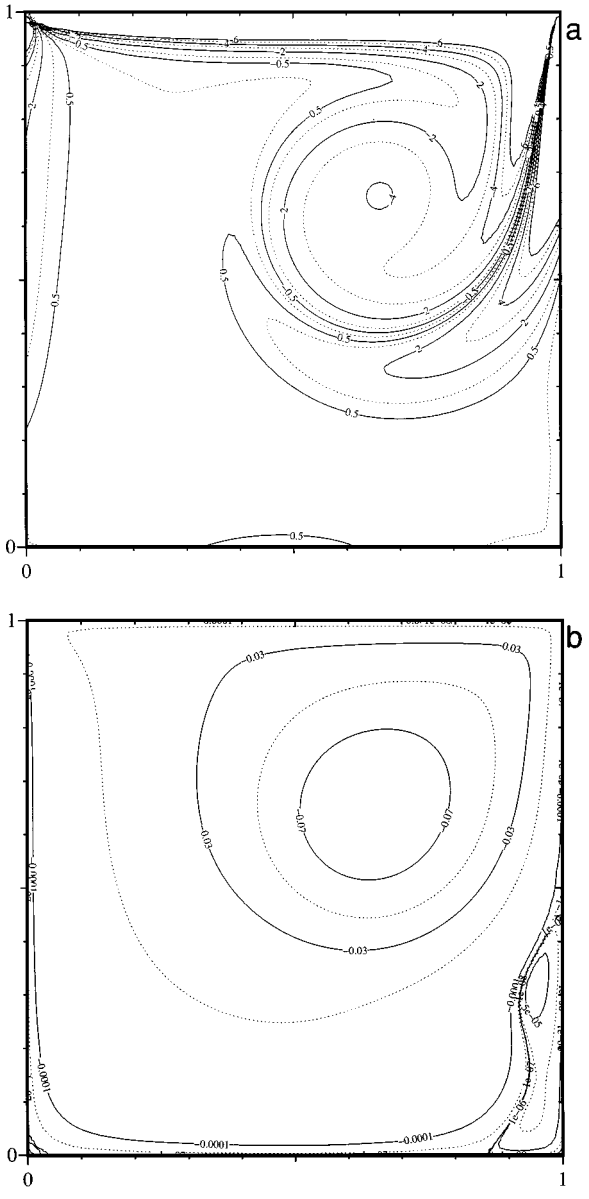

FIG. 6. Finite element solution of the unsteady (unregularized) driven cavity problem with impulsive start for $\mathrm{Re} = 1000$ at $t = 6.25$. Vorticity contours (a) and streamlines (b) using a nonuniform mesh of $\approx 2 \times 80^2$ linear triangles.

The method has been applied to solve the driven cavity problem retained in its original—not regularized—form. The proposed method is found to afford the solution of that singular problem without facing any singularity in the influence matrices. The computed solutions for $\mathrm{Re} = 1000$ using 100 or 150 Legendre modes in both directions agree very well with the reference solution, although a Gibbs' phenomenon is clearly seen, pointing to the exigency of subtracting the corner singularities if the spectral accuracy has to be reached in this non-smooth problem.

The success of the proposed Galerkin spectral approach in the uncoupled solution of the vorticity and stream function equations suggests that it could also be effective in eliminating

spurious singularities of the influence matrix encountered sometimes in other uncoupled formulations of the incompressible Navier–Stokes equations.

REFERENCES

1. E. Anderson *et al.*, *LAPACK* (SIAM, Philadelphia, 1995), 2nd ed.
2. C. Bernardi and Y. Maday, *Approximations spectrales des problèmes aux limites elliptiques* (Springer-Verlag, Paris, 1992).
3. O. Botella and R. Peyret, Benchmark spectral results on the lid-driven cavity flow, *Comput. & Fluids* **27**, 421 (1998).
4. C. Canuto, M. Y. Hussaini, A. Quarteroni, and T. A. Zang, *Spectral Methods in Fluid Mechanics* (Springer-Verlag, New York, 1988).
5. H. J. H. Clercx, A spectral solver for the Navier–Stokes equations in the velocity-vorticity formulation for flows with two nonperiodic directions, *J. Comput. Phys.* **137**, 186 (1997).
6. S. C. R. Dennis and L. Quartapelle, Direct solution of the vorticity-stream function ordinary differential equations by a Chebyshev approximation, *J. Comput. Phys.* **52**, 448 (1983).
7. U. Ehrenstein and R. Peyret, A Chebyshev collocation method for the Navier–Stokes equations with application to double-diffusive convection, I, *J. Numer. Methods Fluids* **9**, 427 (1989).
8. R. Glowinski and O. Pironneau, Numerical methods for the first biharmonic equation and for the two-dimensional Stokes problem, *SIAM Rev.* **12**, 167 (1979).
9. D. Gottlieb and S. O. Orszag, *Numerical Analysis of Spectral Methods: Theory and Applications* (SIAM, Philadelphia, 1977).
10. J.-L. Guermond and L. Quartapelle, Weak approximation of the ψ-ω equations with explicit viscous diffusion, *Math. Models Methods Appl. Sci.*, in press.
11. M. M. Gupta, R. P. Manohar, and B. Noble, Nature of viscous flows near sharp corners, *Comput. & Fluids* **9**, 379 (1981).
12. D. B. Haidvogel and T. A. Zang, The accurate solution of Poisson's equation by expansion in Chebyshev polynomials, *J. Comput. Phys.* **30**, 167 (1979).
13. W. Heinrichs, A spectral multigrid method for the Stokes problem in streamfunction formulation, *J. Comput. Phys.* **102**, 310 (1992).
14. L. Kleiser and U. Schumann, Treatment of the incompressibility and boundary conditions in 3D numerical spectral simulation of plane channel flows, in *Notes on Numerical Fluid Mechanics*, edited by E. H. Hirschel (Vieweg Braunschweig, 1980), pp. 165–173.
15. H. D. Nguyen, S. Paik, and J. N. Chung, Application of vorticity integral conditioning to Chebyshev pseudospectral formulation for the Navier–Stokes equations, *J. Comput. Phys.* **106**, 115 (1993).
16. R. Peyret, Spectral methods for the vorticity–streamfunction equations, in *Computational Fluid Dynamics Review*, edited by M. Hafez and K. Oshima (Wiley, New York, 1997).
17. L. Quartapelle, Vorticity conditioning in the calculation of two-dimensional viscous flows, *J. Comput. Phys.* **40**, 453 (1981).
18. L. Quartapelle, *Numerical Solution of the Incompressible Navier–Stokes Equations* (Birkhäuser, Basel, 1993).
19. A. Quarteroni and A. Valli, *Numerical Approximation of Partial Differential Equations* (Springer-Verlag, Berlin, 1997), 2nd ed.
20. J. Shen, Hopf bifurcation of the unsteady regularized driven cavity, *J. Comput. Phys.* **95**, 228 (1991).
21. J. Shen, Efficient spectral-Galerkin method. I. Direct solvers of second- and fourth-order equations using Legendre polynomials, *SIAM J. Sci. Comput.* **15**, 1489 (1994).
22. J. Shen, Efficient spectral-Galerkin method. II. Direct solvers of second- and fourth-order equations using Chebyshev polynomials, *SIAM J. Sci. Comput.* **16**, 74 (1995).
23. G. Strang and G. J. Fix, *An Introduction to Finite Element Method* (Prentice Hall, Englewood Cliffs, NJ, 1973).